Progress In Electromagnetics Research, Vol. 130, 207–224, 2012

SIERPINSKIZED KOCH-LIKE SIDED MULTIFRACTAL DIPOLE ANTENNA

D. Li* and J. Mao

Key Laboratory of Ministry of Education of China for Research and Design of Electromagnetic Compatibility of High Speed Electronic Systems, Shanghai Jiao Tong University, Shanghai 200240, China

Abstract—Koch-like fractal curve and Sierpinski Gasket are syncretized into a novel Sierpinskized Koch-like sided bow-tie (SKLB) multifractal in superior-inferior way. A K_4S_4 SKLB multifractal dipole fed by a linearly tapered microstrip Balun is designed, simulated, fabricated and measured. The well consistent results from measurement and experiment corroborate validity of design and the multifractal antenna's superiority and advantages over its monofractal counterparts in impedance, bandwidth, directivity, efficiency, and dimension. Six good matched bands ($S_{11} \leq -10\,\mathrm{dB}$) with moderate gain (2.12 dBi–9.55 dBi) and high efficiency (87%–97%) are obtained within band 1.5 GHz–14.5 GHz, of which $f_1 = 1.92\,\mathrm{GHz}$, $f_2 = 3.94\,\mathrm{GHz}$, and $f_3 = 5.09\,\mathrm{GHz}$ are generally useful. The multibands are all almost omnidirectional or quasi-omnidirectional in H-plane ($Phi = 0°$, XOZ) and doughnut-shaped or dented doughnut-shaped in E-plane ($Phi = 90°$, YOZ). So it is an attractive candidate for applications like PCS, IMT2000, UMTS, WLAN, WiFi, WiMAX and other fixed or mobile wireless multiband communication systems.

1. INTRODUCTION

RACTAL antenna has drawn much attention since its introduction in 1995 by Nathan Cohen [1, 2]. It is a combination of antenna technology and fractal geometry [3] and has shown many particular attributes during extensive researches and applications as concluded in [4, 5]. Fractal antenna usually comprises monofractal, which has only one fractal scale ratio, so it essentially has multiband of single frequency ratio [6–8] though with variable scale ratios [9, 10].

Received 1 June 2012, Accepted 2 July 2012, Scheduled 13 August 2012

* Corresponding author: Daotie Li (maplebirchpaeony@yahoo.com.cn).

Naturally, we conceive the idea of fabricating multifractal antenna from several monofractals with different scale ratios, so that we can design arbitrary multiband antennas more easily. Those component monofractals are usually coalesced in superior-inferior or main-minor way. So, multifractal antenna often behaviors like the main monofractal as well as resembles the minor one in impedance property and radiation patterns. It reserves the component monofractals' merits and surmounts their demerits simultaneously. In conclusion, multifractal antenna is closely relevant to the monofractals' properties and their combinative way [11]. Multifractal antenna has brought forth significant advantages over monofractal antenna, such as multiband with multiple frequency ratios, further dimension shrinkage and directivity enhancement [9]. Unfortunately, multifractal hasn't been substantially explored for antenna design. Therefore, it is a promising topic of fractal antennas and deserves to be ulteriorly investigated and developed.

Koch-like curve [12] and Sierpinski Gasket are syncretized in main-minor way, comprising so called Sierpinskized Koch-like sided bow-tie (SKLB) multifractal. A SKLB multfractal dipole fed by a linearly tapered microstrip Balun was designed, optimized, fabricated and measured. Good agreement is acquired between simulation and measurement. Like the KSSG counterpart [11], SKLB multifractal dipole also presents conspicuous multifractal properties in impedance, directivity, efficiency, and dimension. Particularly, it shows more remarkable consistency and conspicuous array effect in radiation patterns.

2. SIERPINSKIZED KOCH-LIKE SIDED BOW-TIE (SKLB)

According to the viewpoints concluded in [11], multifractal usually consists of several monofractals and behaves intimately with the combinative way. Koch-like curve [12] and Sierpinski Gasket are coalesced in superior-inferior way, which is just opposite to that of KSSG multifractal in [11]. For intuitive comprehension of the proposed multifractal, IFS [13, 14] is not adopted for its description. An isosceles triangle (bow-tie) is fractalized with K_i-iterated Koch-like curve on all the sides then a S_j-iterated Sierpinski Gasket with K_n-iterated ($n = 1, 2 \ldots i$) Koch-like sides is hollowed out from the Koch-like fractalized bow-tie, so we obtain K_iS_j Sierpinskized Koch-like sided multifractal bow-tie, called K_iS_j (K_i-Koch-like, S_j-Sierpinski Gasket) SKLB for simplicity, as shown in Fig. 1–Fig. 2. The SKLB multifractal is fully parameterized modeled with Ansoft HFSS$^{\text{TM}}$ v.13. The parameters'

symbols and meanings are as follows: θ_k, θ_s is base angle of the initial isosceles triangle of Koch-like bow-tie and the hollowed initial isosceles triangle of Sierpinski Gasket respectively, φ_k, φ_s is base angle of each iterative isosceles-triangular notch of Koch-like bow-tie and Sierpinski Gasket separately; b_i is rectilinear base side length of un-hollowed vertexal isosceles triangle of the Koch-like bow-tie; d_{Ki} are rectilinear base side length of the lateral K_i-iterated isosceles triangular notches; L_{sj} are rectilinear lateral side lengths of the hollowed isosceles triangles of S_j-iterated Sierpinski Gasket; D_{sj} are rectilinear distance between lateral vertices of the inverted isosceles triangle corresponding to the S_j-iterated hollowed isosceles triangles, which are formed with sharp-angled bulges on the Koch-like fractal sides; μ is height of the Koch-like isosceles triangle bow-tie initiator. All the signs are illustrated, as shown in Fig. 1–Fig. 2. There are some relationships among these arguments:

$$\sigma_{Ki} = \frac{b_{i+1}}{b_i} = \frac{1}{2\cdot(1+\delta_i\cdot\cos\theta_k)} \Leftrightarrow \delta_i = \frac{\left(\frac{1}{2\cdot\sigma_{Ki}}-1\right)}{\cos\theta_k} = \frac{(b_i - 2\cdot b_{i+1})}{2\cdot b_{i+1}\cdot\cos\theta_k}$$

$$b_0 = b_n\cdot 2^n\cdot\prod_{i=1}^{n}(1+\delta i\cdot\cos\theta k)(i=0,1,2\ldots n) \tag{1}$$

$$0 < \rho_{Sj} = \frac{L_{Sj}}{D_{Sj}} < 1, \tag{2}$$

where n is the largest iterative number, σ_{Ki} the ratio of b_{i+1} to b_i and also fractal scale ratio of contiguous iterations of the Koch-like curve, δ_i the ratio of base side length of K_i-iterated notch to rectilinear length of K_i-iterated Koch-like curve, and ρ_{Sj} the ratio of L_{Sj} to D_{Sj}

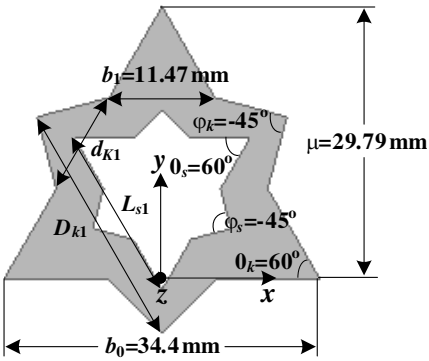

Figure 1. K_1S_1 SKLB, $b_1 = 11.47$ mm.

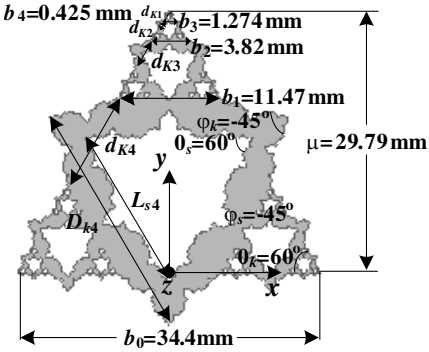

Figure 2. K_4S_4 SKLB, $b_4 = 0.425$ mm.

and also size scale of the hollowed isosceles triangle of S_j-iterated Sierpinski Gasket. Intuitively, it depends upon ρ_{Sj} that how much SKLB multifractal behaves like the main monofractal (Koch-like curve) or resembles the minor one (Sierpinski Gasket) in electrical property. Conspicuously, the Koch-like curve is formed with variable fractal scale ratio among each iterative, which is equal to $\chi^{-1} = \frac{\alpha-1}{2\cdot\alpha}$ in its original literature [11]. So, we get the following relationship:

$$\sigma_{Ki} = \frac{1}{2\cdot(1+\delta_i\cdot\cos\theta_k)} = \frac{\alpha-1}{2\cdot\alpha} \Leftrightarrow \delta_i = \frac{1}{(\alpha-1)\cdot\cos\theta_k}, \tag{3}$$

so the fractal scale ratio of Sierpinski Gasket is:

$$\begin{aligned}\sigma_{Sj} &= \rho_{Sj}\cdot\left[1-\frac{1+\delta_i\cdot\cos(\theta_k-\varphi_k)}{2\cdot(1+\delta_i\cdot\cos\theta_k)\cdot\cos\varphi_k}\right] \\ &= \rho_{Sj}\cdot\{1-\sec\varphi_k\cdot[1+\delta_i\cdot\cos(\theta_k-\varphi_k)]\cdot\sigma_{Ki}\}\end{aligned} \tag{4}$$

If $\sigma_{Sj} = \sigma_{Ki}$, from formula (3) and (4), we get:

$$\begin{aligned}\rho_{Sj} &= \frac{\sigma_{Sj}}{1-\sec\varphi_k\cdot[1+\delta_i\cdot\cos(\theta_k-\varphi_k)]\cdot\sigma_{Ki}} \\ &= \frac{1}{2\cdot(1+\delta_i\cdot\cos\theta_k)-\sec\varphi_k\cdot[1+\delta_i\cdot\cos(\theta_k-\varphi_k)]}\end{aligned} \tag{5}$$

Then from formula (1), (2) and (5), we obtain:

$$\begin{aligned}0<\rho_{Sj}<1 &\Rightarrow 2\cdot(1+\delta_i\cdot\cos\theta_k)\cdot\cos\varphi_k-[1+\delta_i\cdot\cos(\theta_k-\varphi_k)]>\cos\varphi_k \\ &\Rightarrow \cos\varphi_k+\delta_i\cdot\cos(\theta_k+\varphi_k)>1\end{aligned} \tag{6}$$

$$d_{i+1} = d_i \Rightarrow \delta_{i+1} = \frac{\sec\theta_k}{2}\cdot\left(1-\frac{\frac{1}{2}}{1+\delta_i\cdot\cos\theta_k}\right) \tag{7}$$

where α is the ratio of base side length of the protrusive notch isosceles triangle to that of the initiator isosceles triangle b_0, as illustrated in Fig. 2. Here, $\theta_k = \theta_s = 60^\circ$, $\varphi_k = \varphi_s = -45^\circ$, $b_0 = 34.4\,\text{mm}$, $\mu = 29.79\,\text{mm}$, and $\delta_i = 1\,(i = 1, 2, 3\ldots)$ are chosen for good illustration and more convenience. In addition, a more interesting discovery can be found from the multifractal geometry. The discovery is that fractal scale ratio of Koch-like sided Sierpinski Gasket σ_{Sj} is correlated to that of Koch-like curve σ_{Ki} with formula (4), and it is not the classic value 0.5 anymore. But for the KSSG counterpart [11], the two ratios are absolutely independent of each other. Apparently, K_iS_j SKLB multifractal is alterable, which possesses great geometric flexibility and performance adjustability. For example, when $\rho_{Sj} = 0$, $\varphi_k = 0^\circ$, and $\rho_{Sj} = 1$, $\delta_i = 0$, K_iS_j SKLB multifractal metamorphoses into K_i-iterated Koch-like sided bow-tie K_iS_0 and S_j-iterated Sierpinski Gasket K_0S_j separately.

3. K_4S_4 SKLB MULTIFRACTAL DIPOLE ANTENNA

3.1. Physical Design of the Multifractal Dipole

K_4S_4 SKLB multifractal is chosen as a pragmatic antenna solution for remarkable multifractal impedance property, significant size reduction, more enhanced radiation patterns and geometrical simpleness. We endowed the multifractal dipole with a set of optimum parameters yielded by optimization utilities Genetic Algorithm (GA) [15] and Parametric Sweep of Ansoft HFSS^{TM} v.13 Optimetrics as: θ_k =

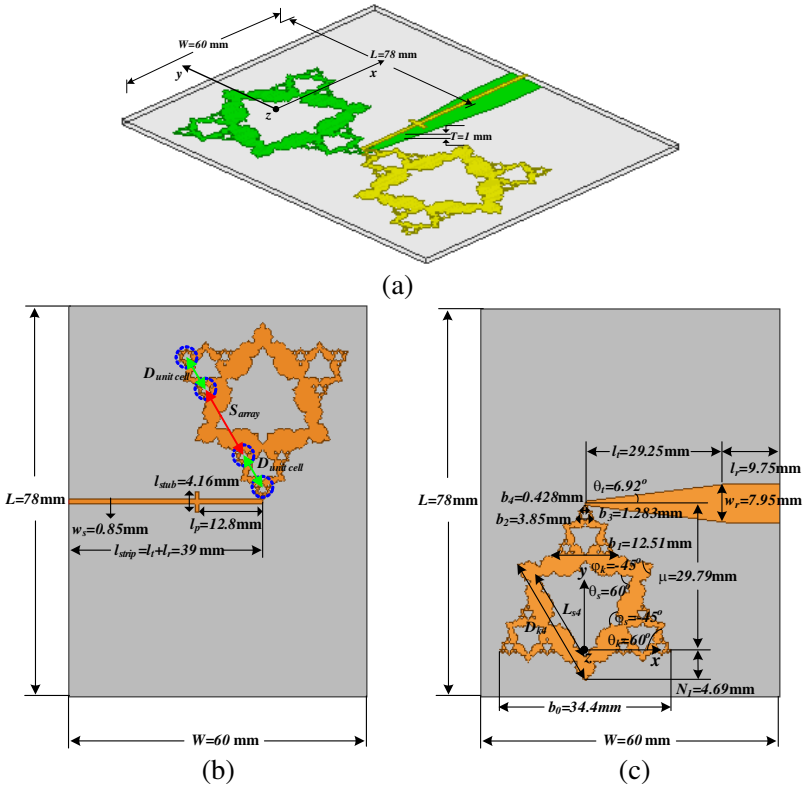

Figure 3. Geometry of K_4S_4 SKLB multifractal dipole (unit: mm). (The parts encircled by blue dotted line are sub self-similar copies of the overall geometry, which comprise unit cells of the array at f_5 = 9.335 GHz, with spacing D_{unit_cell} and sub-array separation S_{array}). (a) Southwest sideview. (yellow-top; green-bottom). (b) Top view. (c) Bottom view.

$\theta_s = 60°$, $\varphi_k = \varphi_s = -45°$; $b_0 = 34.4\,\text{mm}$, $b_1 = 12.51\,\text{mm}$, $b_2 = 3.849\,\text{mm}$, $b_3 = 1.283\,\text{mm}$, $b_4 = 0.4277\,\text{mm}$; because of existence of the joint segment between the vertex and feeding Balun, height of the bow-tie $\mu = 29.79\,\text{mm} + 0.25\,\text{mm} = 30.04\,\text{mm}$; $\delta_1 = \delta_2 = 1$, $\delta_3 = 1.25$, $\delta_4 = 0.75$, $\rho_{sj} = 0.7$. The two arms of the multifractal dipole with a lineally tapered microstrip Balun [16–18] are etched on top and bottom of a Taconic TLX-5A dielectric substrate with size of $78\,\text{mm} \times 60\,\text{mm} \times 1.0\,\text{mm}$ ($L \times W \times T$, with $35\,\mu\text{m}$ copper cladding), $\varepsilon_r = 2.17 \pm 0.02$, and $\tan\delta = 0.0009$ separately, as shown in Fig. 3(a). The balanced ends are connected into the two arms while the unbalanced end is jointed with $50\,\Omega$ SMA connector. The signal trace of the Balun has width $w_s = 0.85\,\text{mm}$ and an orthogonal stub with length $l_{stub} = 4.16\,\text{mm}$ at $l_p = 12.8\,\text{mm}$ away from the feeding joints. The rectilinear segment of the ground of the Balun has length l_r =9.75 mm and width $w_r = 7.95\,\text{mm}$. The linearly tapered segment has length $l_t = 29.25\,\text{mm}$, width $w_t = 7.95\,\text{mm}$–$0.85\,\text{mm}$, and pyramidal angle $\theta_t = 6.92°$, as shown in Figs. 3(b) and 3(c). The overall length and width of the SKLB multifractal dipole is $L = 68.96\,\text{mm}$, $W = 56.2\,\text{mm}$. The multifractal dipole prototype, as shown in Fig. 4, is fabricated by photolightprocess with a photolaser, which emits laser beam with facular diameter of $25\,\mu\text{m}$.

As shown in Fig. 5, simulated input impedance Z_{in} of the K_4S_4 SKLB multifractal dipole displays very consistent values approximating to $50\,\Omega$ at several frequencies within band 1.5 GHz–14.5 GHz, which means remarkable multiband property (red solid-R_{in}, red dash-X_{in}). Accordingly, the simulated reflection coefficient S_{11} is

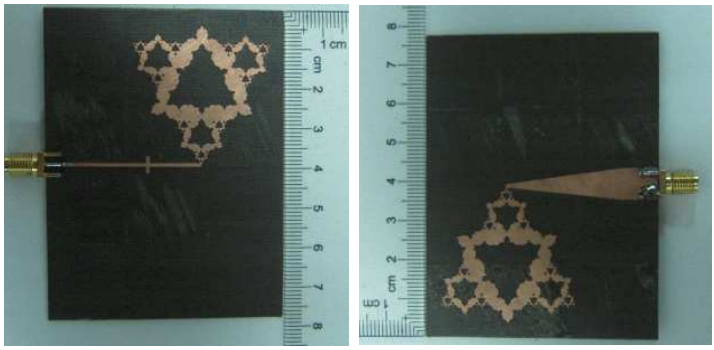

(a) (b)

Figure 4. Prototype of K_4S_4 SKLB multifractal dipole (unit: mm). (a) Top view. (b) Bottom view.

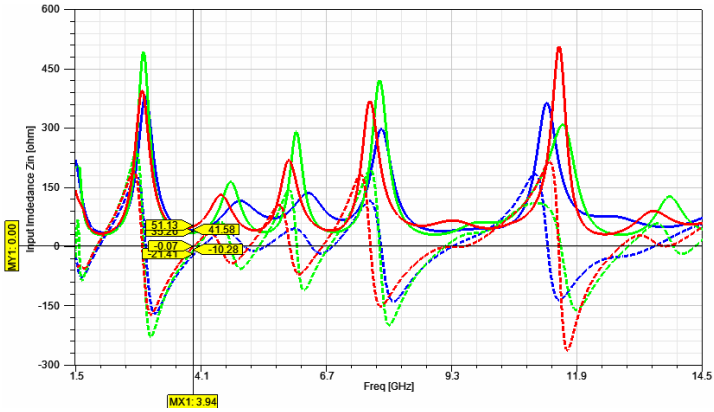

Figure 5. Input impedance Z_{in} of K_iS_j SKLB multifractal dipole (red — K_4S_4, green — K_0S_4, blue — K_4S_0; black-solid — R_{in}; thin dash — X_{in}).

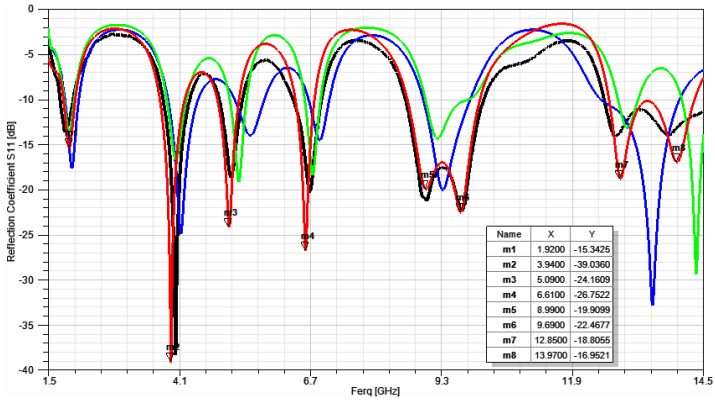

Figure 6. Reflection coefficient S_{11} of K_iS_j SKLB multifractal dipole (red — K_4S_4 simulated, green — K_0S_4, blue — K_4S_0, black — K_4S_4 measured).

shown in Fig. 6 (red solid). It seems that the dipole has eight true resonant frequencies in respect of $S_{11} \leq -15\,\text{dB}$, which corresponds to six bands with $S_{11} \leq -10\,\text{dB}$, of which f_1 is fundamental band, $f_2 - f_5$ are inductive bands during iterative procedure, and f_6 is highest band corresponding to apex intact bow-tie, so the total matched bands: $N = 1 + (i = j = 4) + 1 = 6$ [19]. Then we measured the S_{11} with Agilent E8361C vector network analyzer within the same band, also

as shown in Fig. 6 (black solid). Comparably, the measured (black solid) and simulated (red solid) results of reflection coefficient S_{11} are quite accordant with each other though the former shows higher values and slight shifting at some resonant frequencies. This could be mainly imputed to large ohmic loss of the Balun and copper cladding in high frequency, substrate dielectric permittivity ε_r declination, fabrication tolerance and inherent error of the measurement systems.

3.2. Advantages over the Monofractal Counterparts

In order to ulteriorly reveal the proposed multifractal antenna's superiority over monofractal one in performance, we choose its component fractals K_0S_4 Sierpinski Gasket ($\rho_{Sj} = 1$, $\delta_i = 0$) and K_4S_0 Koch-like sided bow-tie ($\rho_{Sj} = 0$, $\varphi_k = 0^\circ$) as its comparative counterparts because the two fractal dipoles have most similar electrical properties with it. We model the monofractal dipoles identically with the proposed K_4S_4 SKLB multifractal dipole, and simulate them with the same software analysis setups. The simulated and measured results of K_4S_4 SKLB dipole and simulated results of K_0S_4 and K_4S_0 dipoles are merged into corresponding plots for discrepancy comparison and redundancy avoidance, as shown in Figs. 5–15. Thereinto, red, black, green and blue represents simulated and measured K_4S_4, simulated K_0S_4 and K_4S_0 respectively.

As Fig. 5 and Fig. 6 shown, simulated input impedances Z_{in} and reflection coefficients S_{11} of K_4S_4 SKLB dipole (red) alike with that of its monofractal counterparts K_0S_4 Sierpinski Gasket (green) and K_4S_0 Koch-like sided bow-tie (blue). Especially, K_4S_4 resembles the minor component fractal K_0S_4 so much that we are susceptible to doubt the necessity of multifractal. However, the K_4S_4 SKLB multifactal dipole presents lower resonant frequencies, more impedance uniformity and $50\,\Omega$ proximity, which suggests further size reduction and more ideal multiband S_{11}. In addition, all K_iS_j SKLB multifactal dipole manifest conspicuous widebands in high frequency owing to the microstrip Balun. Then we measured the radiation patterns of all the matched bands in a 3D anechoic chamber. The simulated and measured results are merged into corresponding charts for discrepancy comparison and redundancy avoidance, as illustrated in Fig. 7–Fig. 12. In these plots, bold solid, thin dash represents $Phi = 0^\circ$, $Phi = 90^\circ$ principle cut-plane respectively and red, black, green, blue denotes simulated, measured K_4S_4, K_0S_4 and K_4S_0 in sequence.

As shown in Figs. 7–12, measured (black) and simulated (red) results of the gain patterns are also very accordant with each other, but the former have a little asymmetry, which should be attributed to fabrication errors and imperfect test conditions. The maximum

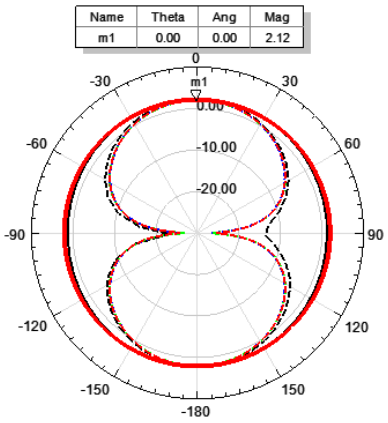

Figure 7. Gain patterns of K_iS_j at f_1 (red — $f_1 = 1.92$ GHz-simulated K_4S_4, black — $f_1 = 1.858$ GHz-measured K_4S_4, green — $f_1 = 1.92$ GHz-K_0S_4, blue — $f_1 = 1.97$ GHz-K_4S_0; solid — $Phi = 0°$-XOZ, dash — $Phi = 90°$-YOZ).

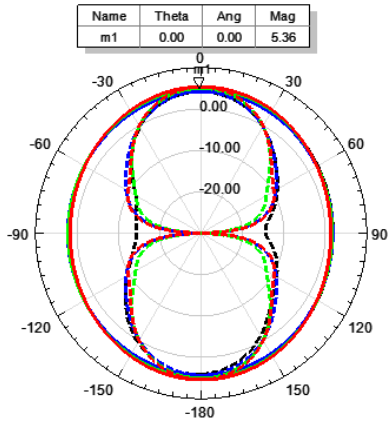

Figure 8. Gain patterns of K_iS_j at f_2 (red — $f_2 = 3.94$ GHz-simulated K_0S_4, black — $f_2 = 4.027$ GHz-measured K_4S_4, green — $f_2 = 4.04$GHz-K_0S_4, blue — $f_2 = 4.13$ GHz-K_4S_0; solid — $Phi = 0°$-XOZ, dash — $Phi = 90°$-YOZ).

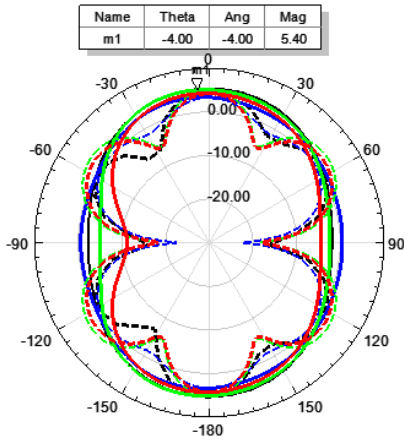

Figure 9. Gain patterns of K_iS_j at f_3 (red — $f_3 = 5.09$ GHz-simulated K_4S_4, black — $f_3 = 5.124$ GHz-measured K_4S_4, green — $f_3 = 5.28$ GHz-K_0S_4, blue — $f_3 = 5.52$ GHz-K_4S_0; solid — $Phi = 0°$-XOZ, dash — $Phi = 90°$-YOZ).

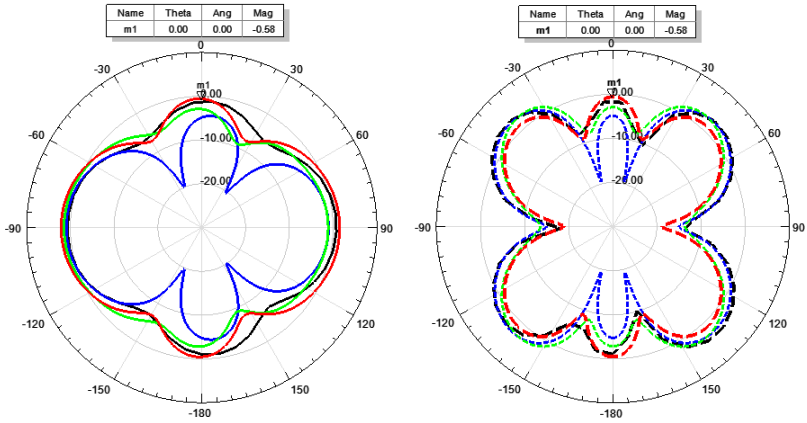

Figure 10. Gain patterns of K_iS_j at f_4 (red — $f_4 = 6.61$ GHz-simulated K_4S_4, black — $f_4 = 6.684$ GHz-measured K_4S_4, green — $f_4 = 6.75$ GHz-K_0S_4, blue — $f_3 = 6.89$ GHz-K_4S_0). (a) $Phi = 0°$-XOZ. (b) $Phi = 90°$-YOZ.

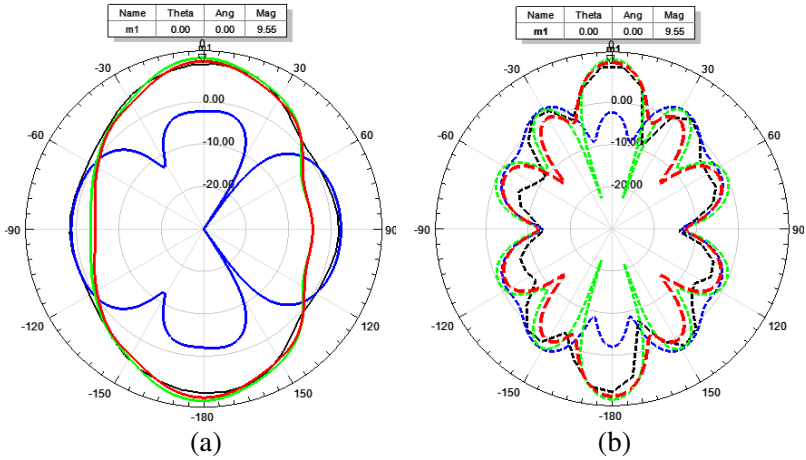

Figure 11. Gain patterns of K_iS_j at f_5 (red — $f_5 = 9.335$,GHz-simulated K_4S_4, black — $f_5 = 9.333$,GHz-measured K_4S_4, green — $f_5 = 9.23$,GHz-K_0S_4, blue — $f_5 = 9.34$ GHz-K_4S_0). (a) $Phi = 0°$-XOZ. (b) $Phi = 90°$-YOZ.

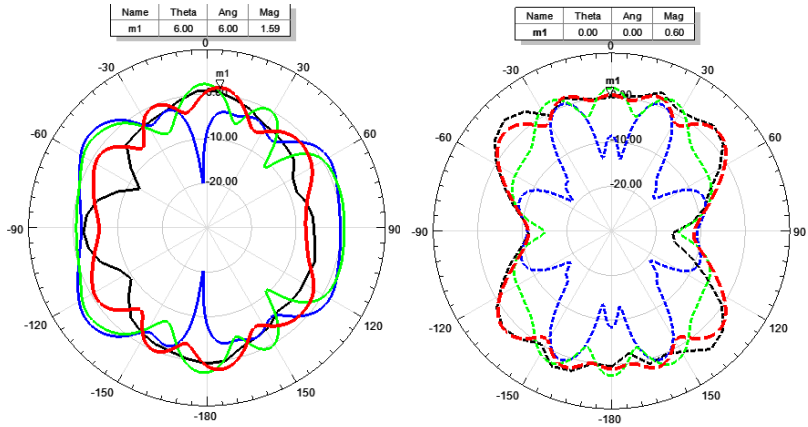

Figure 12. Gain patterns of K_iS_j at f_6 (red — $f_6 = 13.41$ GHz-simulated K_4S_4, black — $f_6 = 13.24$ GHz-measured K_4S_4, green — $f_6 = 13.67$ GHz-K_0S_4, blue — $f_6 = 13.48$ GHz-K_4S_0). (a) $Phi = 0°$-XOZ. (b) $Phi = 90°$-YOZ.

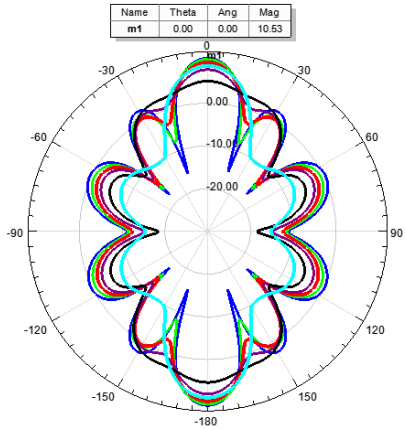

Figure 13. E-plane ($Phi = 90°$-YOZ) gain patterns of K_4S_4 SKLB multifractal dipole at $f_5 = 9.335$ GHz with sweep of δ_3 ($G_{\max} = 10.53$ dBi; blue — $\delta_4 = 0.6$, green — $\delta_4 = 0.8$, red — $\delta_4 = 1.0$, purple — $\delta_4 = 1.2$, black — $\delta_4 = 1.4$, cyan — $\delta_4 = 1.6$)

radiations are in the vicinity of the normal direction ($+Z$). In addition, similarity and asymmetry are also observed from the simulated patterns. Gain patterns of K_4S_4 SKLB dipole at f_1 and f_2 are omnidirectional in XOZ ($Phi = 0°$, H-plane) and doughnut-shaped

in YOZ ($Phi = 90°$, E-plane), as shown in Figs. 7, 8. Gain patterns of K_4S_4 SKLB dipole at f_3 and f_4 are quasi-omnidirectional in XOZ ($Phi = 0°$, H-plane), cloven doughnut-shaped or dented doughnut-shaped in YOZ ($Phi = 90°$, E-plane), as shown in Figs. 9, 10. Gain patterns of K_4S_4 SKLB dipole at f_5 are elliptoid (with long axis in Z-axis) in XOZ (Phi =0°, H-plane), cloven doughnut-shaped in YOZ (Phi =90°, E-plane), as shown in Fig. 11. Gain of f_5, which is as high as 9.55 dBi, indicates that there is a broadside array formed by self-similar elements with smaller scale in this multifractal geometry, as depicted in Fig. 3(b). For validity of this viewpoint, parametric sweep is undertook for δ_4, which is the most relevant parameter to f_5, and side lobe level of the gain pattern in E-plane decreases with δ_4 distinctly, which indicates that the pattern closely correlates to element spacing, excitation amplitude, and phase discrepancy just like its conventional counterpart half-wavelength broadside dipole array (4 unit cells spaced about 0.8–0.9λ), as illustrated in Fig. 13. For optimal synthesis of gain pattern, the four lateral unit cells should be equidistant, namely $D_{unit\_cell} = S_{array}$, so from formula (7), we acquire: $\theta_k = 60°$, $\delta_3 = 1$, $\delta_4 = 2/3$. From Fig. 13, we can see that $\delta_4 = 0.6$ is very approximate to this optimum value. Such array with element coalition and inequable excitation should be a very peculiar phenomenon emerging in multifractal antenna.

Gain patterns of K_4S_4 at f_6 are also elliptoid (with long axis in Z-axis) in XOZ ($Phi = 0°$, H-plane), rippled doughnut-shaped in YOZ ($Phi = 90°$, E-plane), as shown in Fig. 12.

Such radiation patterns above suggest that K_4S_4 SKLB dipole operates as a half-wavelength dipole at all matched bands except $f_4(\approx 1.5 \times \lambda)$. It doesn't present identical gain patterns in multiband as the standard half-wavelength dipole due to fringe or end effect [20] of the smaller scale parts corresponding to the whole fractal similar geometry. Slight asymmetry of gain patterns could be attributed to the antipodal configuration, the feedline's $+X$ extension and noideal $\pm 180°$ phase difference at balanced ends of the Balun.

Gain patterns of K_4S_4 SKLB dipole very resembles that of K_0S_4 and K_4S_0 in low frequency, as shown in Figs. 7–9, but it displays a little improved gains than K_0S_4 and enhances distinctly than K_4S_0, which maximizes in $-X$ direction in H-plane and nulls in Z direction in high frequency, as shown in Fig. 10–Fig. 12. Analogical gain patterns of multibands indicate SKLB dipole's better identity in radiation than monofractal counterparts like [11] and [12]. Likewise, remarkable enhancements like higher gain and better directivity over its component monofractals K_4S_0 and K_0S_4 are acquired for these multiband patterns. The K_4S_4 SKLB dipole behaves more like K_0S_4

Sierpinski Gasket within the overall band though this monofractal is arranged in inferior order. The fact indicates that it's the panoramic monofractal rather than the local monofractal dominates the mutlifractal's properties.

For convenient acquisition of thorough properties, the simulated resonant results are tabulated in Table 1.

As shown in Table 1, f_1, f_2 and f_3 just fall upon very useful bands with considerable relative bandwidth such as UMTS, WiFi, and WiMAX, which means K_4S_4 SKLB dipole will be a competitive multiband antenna candidate at least a triband antenna with better

Table 1. Simulated resonant properties of K_iS_j SKLB multifractal dipole.

	f_i (GHz)	f_1	f_2	f_3
		1.92	3.94	5.09
	f_{n+1}/f_n	-	**2.052**	**1.292**
K_4S_4	R_{in} (Ω)	35.76	51.13	44.52
	S_{11} (dB)	-15.34	-39.04	-24.16
	BW (MHz)	242, 12.61%	510, 12.95%	460, 9.04%
	Gain (dBi)	2.12	5.36	5.40
	f_i (GHz)	f_1	f_2	f_3
		1.92	4.04	5.28
	f_{n+1}/f_n	-	**2.104**	**1.307**
K_0S_4	R_{in} (Ω)	33.21	37.80	40.62
	S_{11} (dB)	-13.69	-17.93	-19.16
	BW (MHz)	200, 10.42%	391, 9.68%	336, 6.36%
	Gain (dBi)	2.04	5.04	5.06
	f_i (GHz)	f_1	f_2	f_3
		1.97	4.13	5.52
	f_{n+1}/f_n	-	**2.096**	**1.337**
K_4S_0	R_{in} (Ω)	41.53	44.77	73.69
	S_{11} (dB)	-17.60	-24.88	-14.0
	BW (MHz)	275, 13.96%	600, 14.53%	600, 10.87%
	Gain (dBi)	2.08	4.28	3.36

K_4S_4	f_i (GHz)	f_4	f_5	f_6
		6.61	9.335 (8.99–9.68)	13.41 (12.85–13.97)
	f_{n+1}/f_n	**1.299**	**1.412**	**1.437**
	R_{in} (Ω)	45.68	59.29	41.50
	S_{11}(dB)	−26.75	−19.91	−18.81
	BW (MHz)	400, 6.05%	1460, 15.62%	1730, 12.85%
	Gain (dBi)	1.50	9.55	1.59
K_0S_4	f_i (GHz)	f_4	f_5	f_6
		6.75	9.23	13.67 (12.99–14.35)
	f_{n+1}/f_n	**1.278**	**1.367**	**1.481**
	R_{in} (Ω)	39.29	35.16	32.53
	S_{11} (dB)	−18.37	−14.32	−13.17
	BW(MHz)	318, 4.71%	868, 9.41%	1013, 7.41%
	Gain (dBi)	−2.94	10.28	2.26
K_4S_0	f_i (GHz)	f_4	f_5	f_6
		6.89	9.34	13.48
	f_{n+1}/f_n	**1.248**	**1.356**	**1.443**
	R_{in} (Ω)	71.54	41.19	52.30
	S_{11}(dB)	−14.50	−19.97	−32.80
	BW (MHz)	416, 6.04%	933, 9.99%	1569, 11.64%
	Gain (dBi)	−4.87	−2.27	−8.54

gain patterns and higher gains than that of [21–25] at f_1, f_2, and f_3 respectively, for many wireless communication applications; larger percentage bandwidths than K_0S_4 and K_4S_0 at f_5 and f_6 validate band widening property of the proposed multifractal; resonant impedances R_{in} are all very approximate to $50\,\Omega$ and reflection coefficients S_{11} are all less than $-15\,$dB, which suggest conspicuous multifractal impedance uniformity; adjacent frequency ratio presents remarkable multi-values and consistency, which denotes distinct multifractal multiband characteristics.

At the end, the radiation efficiency of f_1, f_2 and f_3 are measured

and tabulated in Table 2.

Table 2. Measured gain and efficiency of f_1, f_2 and f_3 (E, H-plane).

f (GHz)	Gain (E, dBi)	HPBW (E, °)	Gain (H, dBi)	HPBW (H, °)	Effic (η)
1.88	2.04	79.0	2.04	-	96%
1.92	2.10	78.5	2.10	-	97%
1.96	2.07	78.5	2.07	-	95%
3.90	4.57	32	4.57	-	92%
3.94	4.50	32	4.50	-	92%
3.98	4.55	33	4.55	-	92%
5.05	5.32	21.6	5.32	60.5	86%
5.09	5.36	21	5.36	61	87%
5.14	5.43	22	5.43	60	87%

As Table 2 shown, the radiation efficiency η at the test bands is high and decreases with f, because loss increases with frequency. In conclusion, the K_4S_4 SKLB multifractal dipole does not degrade with iteration growth and frequency increase in performance like bandwidth, gain and efficiency.

4. CONCLUSION

Koch-like curve and Sierpinski Gasket are coalesced into a fire-new Sierpinskized Koch-like sided bow-tie multifractal (SKLB) in main-minor way with correlative and variable fractal scale ratios [26]. A K_4S_4 SKLB multifractal dipole with variable fractal sale ratios fed by a linearly tapered microstrip Balun, etched on a Taconic TLX-5A dielectric substrate with dimension of 78 mm (68.96 mm) × 60 mm (56.2 mm) × 1.0 mm ($L \times W \times T$, with 35 µm copper cladding), $\varepsilon_r = 2.17 \pm 0.02$, and $\tan\delta = 0.0009$, is designed, simulated, fabricated and measured. If a higher permittivity substrate, such as FR4, is chosen, more compact configuration will be obtained [27], so that it will be suitable for small multiband wireless device such as RFID [28] and USB dongle [29]. The well accordant results from measurement and experiment corroborate validity of the design with Ansoft HFSS^{TM} v.13 and the multifractal antenna's superiority and advantages over its monofractal counterparts in impedance uniformity, bandwidth broadening, directivity amelioration, dimension shrinkage, and efficiency enhancement. Six well matched bands ($S_{11} \leq -10$ dB) with moderate gain (2.12 dBi–9.55 dBi) and high efficiency (87%–97%)

are obtained within band 1.5 GHz–14.5 GHz, and all the bands $f_1 =$ 1.92 GHz (1.8 GHz–2.042 GHz; 242 MHz, 12.61%, PCS1900 + UMTS), $f_2 =$ 3.94 GHz (3.71 GHz–4.22 GHz; 510 MHz, 12.95%, WiMAX), $f_3 =$ 5.09 GHz (4.84 GHz–5.3 GHz; 460 MHz, 9.04%, WiMAX), $f_4 =$ 6.61 GHz (6.4 GHz–6.8 GHz; 400 MHz, 6.05%), $f_5 =$ 9.335 GHz (8.62 GHz–10.08 GHz; 1460 MHz 15.62%), $f_6 =$ 13.41 GHz (12.6 GHz–14.33 GHz; 1730 MHz, 12.85%), in which peculiar array effect is observed, are generally useful. The multibands are omnidirectional or quasi-omnidirectional in H-plane ($Phi = 0°$, XOZ) and doughnut-shaped or dented doughnut-shaped in E-plane ($Phi = 90°$, YOZ). Moreover, this multifractal antenna possesses compactness, simpleness, and lightweight. So it is an attractive candidate for applications such as PCS, IMT2000, UMTS, WLAN, WiFi, WiMAX and other fixed or mobile wireless multiband communication systems [30].

ACKNOWLEDGMENT

This work was supported by the National Basic Research Program of China under Grant of 2009CB320202. The authors are very grateful to Prof. Kuai from National Key Lab of Millimeter Waves, Southeast University of China and Qinfang Li from Suzhou R&D Center of Huizhou Speed Communication Technology Co, Ltd. for radiation pattern measurement.

REFERENCES

1. Cohen, N., "Fractal antennas: Part 1," *Communications Quarterly*, 7–22, Aug. 1995.
2. Cohen, N., "Fractal antenna applications in wireless telecommunications," *IEEE Electronics Industries Forum of New England*, 43–49, May 1997.
3. Werner, D. H., R. L. Haup, and P. L. Werner, "Fractal antenna engineering: The theory and design of fractal antenna arrays," *IEEE Antennas and Propagation Magazine*, Vol. 41, No. 5, 37–58, Oct. 1999.
4. Anguera, J., C. Puente, C. Borja, and J. Soler, "Fractal-shaped antennas: A review," *Wiley Encyclopedia of RF and Microwave Engineering*, Vol. 2, 1620–1635, Apr. 2005.
5. Liu, Y., S. Gong, and D. Fu, "The advances in development of fractal antennas," *Chinese Journal of Radio Science*, Vol. 17, No. 1, Feb. 2002.
6. Kaur, J., S. Singh, and A. Kansal, "Multiband behavior of

Sierpinski fractal antenna," *Res. J. Inform. Technol.*, Vol. 3, No. 1, 35–43, Mar. 2011.

7. Sinha, S. N. and M. Jain, "A self-affine fractal multiband antenna," *IEEE Antennas and Wireless Propagation Letters*, Vol. 6, 110–112, Apr. 2007.
8. Rathee, D. and J. Ashraf, "CPW-fed Sierpinski fractal monopole antenna with varying scale factor," *International Journal of Electronics Engineering*, Vol. 3, No. 1, 77–80, 2011.
9. Hwang, K. C., "A modified Sierpinski fractal antenna for multiband application," *IEEE Antennas and Wireless Propagation Letters*, Vol. 6, 357–360, May 2007.
10. Manimegalai, B., S. Raju, and V. Abhaikumar, "A multifractal Cantor antenna for multiband wireless applications," *IEEE Antennas and Wireless Propagation Letters*, Vol. 8, 359–362, Aug. 2009.
11. Li, D. and J. Mao, "Koch-like sided Sierpinski Gasket multifractal dipole antenna," *Progress In Electromagnetics Research*, Vol. 126, 399–427, 2012.
12. Li, D. and J. Mao, "A Koch-like sided bow-tie fractal dipole antenna," *IEEE Trans. on Antennas and Propaga.*, Vol. 60, No. 5, 40–49, May 2012.
13. Mandelbrot, B. B., *The Fractal Geometry of Nature*, 2nd Edition, W. H. Freeman, New York, 1983.
14. Falconer, K., *Fractal Geometry: Mathematical Foundations and Applications*, 2nd Edition, John Wiley&Son, Inc, New York, 2003.
15. Zhu, X., W. Shao, J.-L. Li, and Y.-L. Dong, "Design and optimization of low RCS patch antennas based on a genetic algorithm," *Progress In Electromagnetics Research*, Vol. 122, 327–339, 2012.
16. Dey, S., C. K. Aanandan, K. A. Jose, and P. Monahan, "Wideband printed dipole antenna," *Microwave and Optical Technology Letters*, Vol. 4, No. 10, 417–419, Sep. 1991.
17. Chen, G. Y. and J. S. Sun, "A printed dipole antenna with microstrip tapered Balun," *Microwave and Optical Technology Letters*, Vol. 40, No. 4, 344–346, Feb. 2004.
18. Eldek, A. A., "Design of double dipole antenna with enhanced usable bandwidth for wideband phased array applications," *Progress In Electromagnetics Research*, Vol. 59, 1–15, 2006.
19. Puente, C., J. Romeu, R. Pous, and A. Cardama, "On the behavior of the Sierpinski multiband fractal antenna," *IEEE Trans. on Antennas and Propaga.*, Vol. 46, 517–524, Apr. 1998.

20. Heldring, A., E. Ubeda, and J. M. Rius, "Efficient computation of the effect of wire ends in thin wire analysis," *IEEE Trans. on Antennas and Propaga.*, Vol. 54, No. 10, 3034–3037, Oct. 2006.
21. Mahatthanajatuphat, C., S. Saleekaw, P. Akkaraekthalin, and M. Krairiksh, "A rhombic patch monopole antenna with modified Minkowski fractal geometry for UMTS, WLAN, and mobile WiMAX application," *Progress In Electromagnetics Research*, Vol. 89, 57–74, 2009.
22. Lizzi, L. and G. Oliveri, "Hybrid design of a fractal-shaped GSM/UMTS antenna," *Journal of Electromagnetic Waves and Applications*, Vol. 24, No. 5–6, 707–719, 2010.
23. Li, C.-M., K. Wang, and C.-K. Chen, "Small tri-band monopole antenna for WIMAX/WLAN applications," *Journal of Electromagnetic Waves and Applications*, Vol. 25, No. 8–9, 1297–1307, 2011.
24. He, K., R.-X. Wang, Y.-F. Wang, and B.-H. Sun, "Compact tri-band claw-shaped monopole antenna for WLAN/WIMAX applications," *Journal of Electromagnetic Waves and Applications*, Vol. 25, No. 5–6, 869–877, 2011.
25. Weng, W.-C. and C.-L. Hung, "Design and optimization of a logo-type antenna for multiband applications," *Progress In Electromagnetics Research*, Vol. 123, 159–174, 2012.
26. Song, C. T. P., P. S. Hall, and H. Ghafouri-Shiraz, "Perturbed Sierpinski multiband fractal antenna with improved feeding technique," *IEEE Trans. on Antennas and Propaga.*, Vol. 51, No. 5, 1011–1017, May 2003.
27. Panda, J. R. and R. S. Kshetrimayum, "A printed 2.4 GHz/5.8 GHz dual-band monopole antenna with a protruding stub in the ground plane for WLAN and RFID applications," *Progress In Electromagnetics Research*, Vol. 117, 425–434, 2011.
28. Amin, Y., Q. Chen, H. Tenhunen, and L.-R. Zheng, "Performance-optimized quadrate bowtie RFID antennas for cost-effective and eco-friendly industrial applications," *Progress In Electromagnetics Research*, Vol. 126, 49–64, 2012.
29. Ban, Y.-L., J.-H. Chen, S.-C. Sun, J. L.-W. Li, and J.-H. Guo, "Printed wideband antenna with chip-capacitor-loaded inductive strip for LTE/GSM/UMTS WWAN wireless USB dongle applications," *Progress In Electromagnetics Research*, Vol. 128, 313–329, 2012.
30. Moradi, K. and S. Nikmehr, "A dual-band dual-polarized microstrip array antenna for base stations," *Progress In Electromagnetics Research*, Vol. 123, 527–541, 2012.